

Spin-polarized Specular Andreev Reflections in Altermagnets

Yutaro Nagae,^{1,*} Andreas P. Schnyder,² and Satoshi Ikegaya^{1,3,*}

¹*Department of Applied Physics, Nagoya University, Nagoya 464-8603, Japan*

²*Max-Planck-Institut für Festkörperforschung, Heisenbergstrasse 1, D-70569 Stuttgart, Germany*

³*Institute for Advanced Research, Nagoya University, Nagoya 464-8601, Japan*

(Dated: May 28, 2024)

We propose a multi-terminal device consisting of an s -wave superconductor coupled to an altermagnet, to generate highly correlated spin currents via Cooper pair splitting. Remarkably, we find that the correlated spin currents are induced by specular Andreev reflections in the altermagnet, an effect that has up to now been predicted to occur only in a very limited number of systems, e.g., Dirac/Weyl materials coupled to superconductors. We demonstrate that positive non-local charge currents and positive noise cross-correlations are unambiguous fingerprints of the specular Andreev reflections in our proposed device.

Introduction. The combination of magnetism and superconductivity has been a fruitful source of novel phenomena in condensed matter physics [1–4]. The recent discovery of altermagnets (AMs) [5–14], in which spin split bands coexist with compensated collinear magnetic order, has enormously stimulated research in this field. For example, Andreev reflections [15–17], proximity effects [18–20], Josephson effects [21–23], superconducting diode effects [24], superconducting spin-splitter effects [25], and topological superconductivity [26–29] in AM–superconductor (SC) hybrid devices have been reported in a very short time after the discovery of altermagnets.

In this Letter, we discuss nonlocal transport properties in a hybrid device consisting of an AM, an s -wave SC, and two normal-metal leads, as illustrated in Fig. 1. Remarkably, we find that the characteristic magnetic nature of the AM causes specular Andreev reflections (SARs) [30], while usual retro-Andreev reflections are extremely suppressed. Importantly, SAR leads to Cooper pair splitting generating spin-entangled electron pairs [31–43], which has important potential applications in quantum information processing [44, 45]. The SAR has been predicted up to now only for a very limited number of systems, namely for certain Dirac or Weyl materials coupled to superconductors [46–64]. Here, we present an alternative promising route to observe SAR, namely a device in which an s -wave superconductor is couple to an altermagnet. We demonstrate that positive nonlocal charge currents [65] and positive noise cross-correlations [31, 32] are unambiguous observable signatures of the SARs in the present device. Remarkably, thanks to the unique magnetic properties of AMs, the SAR in the present device intrinsically generates entangled spin currents: the currents in the biased lead are carried by electrons with up (down) spins, while the currents in the grounded lead are carried by holes with down (up) spins, as shown in Fig. 2. Note that to generate correlated spin currents by the SARs in Dirac/Weyl-material based devices, ferromagnetic leads with anti-parallel magnetic moments are required to generate an

imbalance between the spins [47, 50, 65–68]. Therefore, the proposed AM-SC hybrid device, which naturally generates spin currents through spin-polarized SAR in the AM, is a highly efficient Cooper pair splitter and generator of entangled spin-currents.

Model and Formulation. We consider the AM-SC hybrid device illustrated in Fig. 1 on a two-dimensional tight-binding model. To describe the two normal-metal leads and the SC, we consider a square lattice, where we set the lattice constant a_0 to one. The different lattice sites are denoted by $\mathbf{r} = j\mathbf{x} + m\mathbf{y}$, where \mathbf{x} (\mathbf{y}) is the unit vector in the x (y) direction. The s -wave SC occupies the lattice sites with $j > L$ and $1 \leq m \leq W$. The first (second) normal-metal occupies the lattice sites with $j < 1$ and $1 \leq m \leq W_n$ ($W - W_n + 1 \leq m \leq W$). In the y directions, we assume open boundary conditions, while in the x direction we consider a semi-infinite superconductor and semi-infinite leads. The Bogoliubov-de Gennes

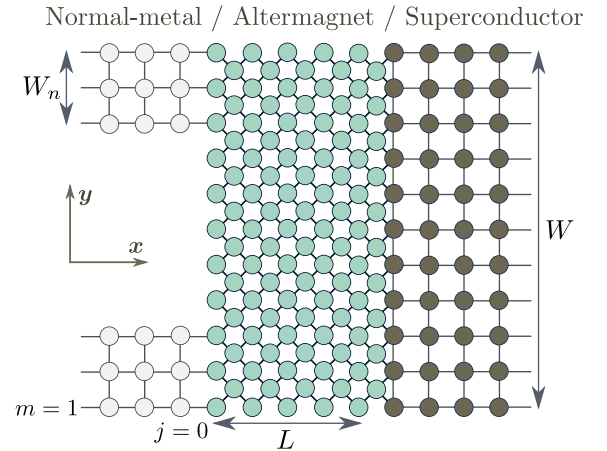


FIG. 1. Schematic image of the device consisting of the AM, s -wave SC, and two normal-metal leads.

Hamiltonian for the SC is given by,

$$H_{\text{SC}} = \frac{1}{2} \sum_{\mathbf{r}, \mathbf{r}' \in \text{SC}} \sum_{\sigma} \Psi_{\mathbf{r}\sigma}^{\dagger} \begin{pmatrix} \xi_{\mathbf{r}, \mathbf{r}'} & s_{\sigma} \Delta_{\mathbf{r}, \mathbf{r}'} \\ s_{\sigma} \Delta_{\mathbf{r}, \mathbf{r}'} & -\xi_{\mathbf{r}, \mathbf{r}'} \end{pmatrix} \Psi_{\mathbf{r}'\sigma},$$

$$\xi_{\mathbf{r}, \mathbf{r}'} = -t\delta_{|\mathbf{r}-\mathbf{r}'|,1} - \mu\delta_{\mathbf{r}, \mathbf{r}'}, \quad \Delta_{\mathbf{r}, \mathbf{r}'} = \Delta\delta_{\mathbf{r}, \mathbf{r}'}, \quad (1)$$

where $\Psi_{\mathbf{r}\sigma} = (c_{\mathbf{r}, \sigma}, c_{\mathbf{r}, \bar{\sigma}}^{\dagger})^{\text{T}}$ with $c_{\mathbf{r}, \sigma}^{\dagger}$ ($c_{\mathbf{r}, \sigma}$) representing the creation (annihilation) operator of an electron at site \mathbf{r} with spin σ (\uparrow or \downarrow); t is the nearest-neighbor hopping integral, μ denotes the chemical potential, and Δ is the pair potential. $\sum_{\mathbf{r}, \mathbf{r}' \in \text{SC}}$ represents the summation over the lattice sites in the SC segment, $\bar{\sigma}$ represents the opposite spin of σ , and $s_{\sigma} = +1(-1)$ for $\sigma = \uparrow$ (\downarrow). We describe the α -th normal-metal lead (N_{α}) by

$$H_{N_{\alpha}} = \frac{1}{2} \sum_{\mathbf{r}, \mathbf{r}' \in N_{\alpha}} \sum_{\sigma} \Psi_{\mathbf{r}\sigma}^{\dagger} \begin{pmatrix} \xi_{\mathbf{r}, \mathbf{r}'} & 0 \\ 0 & -\xi_{\mathbf{r}, \mathbf{r}'} \end{pmatrix} \Psi_{\mathbf{r}'\sigma}, \quad (2)$$

where $\sum_{\mathbf{r}, \mathbf{r}' \in N_{\alpha}}$ represents the summation over the lattice sites belonging to the lead N_{α} . For the AM segment, we assume a metallic AM with a d_{xy} -wave magnetic order, for which RuO_2 is a promising candidate material. It has been theoretically [6, 8, 10] and experimentally [14] shown that RuO_2 has characteristic spin-polarized Fermi surfaces, as shown in Fig. 2. Specifically, in the vicinity of $k_z = 0$ (with k_z being the momentum along the z crystal axis), the spin- \uparrow [spin- \downarrow] Fermi surfaces of RuO_2 have an open shape along the $(k_x + k_y)$ -direction [$(k_x - k_y)$ -direction], as shown in Fig. 2(a) [Fig. 2(b)]. To reproduce such spin-polarized open Fermi surfaces, we employ an effective single-band model with a d_{xy} -wave altermagnetic order, where the Hamiltonian in momentum space

is given by [10, 19, 21],

$$H_{\text{AM}} = \sum_{\mathbf{k}, \sigma} (\varepsilon_{\mathbf{k}} - \mu_0 + s_{\sigma} m_{\mathbf{k}}) c_{\mathbf{k}\sigma}^{\dagger} c_{\mathbf{k}\sigma},$$

$$\varepsilon_{\mathbf{k}} = 2t_0 \cos \frac{k_x}{2} \cos \frac{k_y}{2}, \quad m_{\mathbf{k}} = 2t_J \sin \frac{k_x}{2} \sin \frac{k_y}{2}, \quad (3)$$

where $c_{\mathbf{k}\sigma}^{\dagger}$ ($c_{\mathbf{k}\sigma}$) is the creation (annihilation) operator of an electron with momentum \mathbf{k} and spin σ ; t_0 denotes the nearest-neighbor hopping integral on the square-lattice tilted at 45° with a lattice constant $1/\sqrt{2}$ (see Fig. 1), μ_0 is the chemical potential, and t_J is the strength of the d_{xy} -wave exchange potential. For $|\mu_0| < 2t_J$ with $t_J \leq t_0$ and for $|\mu_0| < 2t_0$ with $t_J \geq t_0$, the effective model in Eq. (3) exhibits the open Fermi surfaces as shown in Fig. 2. Otherwise, we obtain closed Fermi surfaces surrounding the high-symmetry points of the Brillouin zone; see also the Supplemental Material [69]. In real space, the lattice sites of the effective AM model are located at $\mathbf{r} = j\mathbf{x} + m\mathbf{y}$ and $\mathbf{r} = j'\mathbf{x} + m'\mathbf{y} + (\mathbf{x} + \mathbf{y})/2$, as illustrated in Fig. 1. In the x (y) direction, the AM occupies $1 \leq j \leq L$ ($1 \leq m \leq W$) and $1 \leq j' \leq L$ ($1 \leq m' \leq W - 1$). The Hamiltonian in real space is given by

$$H_{\text{AM}} = \frac{1}{2} \sum_{\mathbf{r}, \mathbf{r}' \in \text{AM}} \sum_{\sigma} \Psi_{\mathbf{r}\sigma}^{\dagger} \begin{pmatrix} \xi_{\mathbf{r}, \mathbf{r}'}^{\sigma} & 0 \\ 0 & -\xi_{\mathbf{r}, \mathbf{r}'}^{\bar{\sigma}} \end{pmatrix} \Psi_{\mathbf{r}'\sigma},$$

$$\xi_{\mathbf{r}, \mathbf{r}'}^{\sigma} = \varepsilon_{\mathbf{r}, \mathbf{r}'} - \mu_0 \delta_{\mathbf{r}, \mathbf{r}'} + s_{\sigma} m_{\mathbf{r}, \mathbf{r}'}, \quad (4)$$

$$\varepsilon_{\mathbf{r}, \mathbf{r}'} = \frac{t_0}{2} \left\{ \delta_{\mathbf{r} + \frac{\mathbf{x} + \mathbf{y}}{2}, \mathbf{r}'} + \delta_{\mathbf{r} + \frac{\mathbf{x} - \mathbf{y}}{2}, \mathbf{r}'} + (\mathbf{r} \leftrightarrow \mathbf{r}') \right\},$$

$$m_{\mathbf{r}, \mathbf{r}'} = -\frac{t_J}{2} \left\{ \delta_{\mathbf{r} + \frac{\mathbf{x} + \mathbf{y}}{2}, \mathbf{r}'} - \delta_{\mathbf{r} + \frac{\mathbf{x} - \mathbf{y}}{2}, \mathbf{r}'} + (\mathbf{r} \leftrightarrow \mathbf{r}') \right\},$$

where $\sum_{\mathbf{r}, \mathbf{r}' \in \text{AM}}$ denotes the summation over the lattice sites in the AM. The interface between the lead N_{α} and AM and the interface between the AM and SC are described by

$$H_{\text{AM}-N_{\alpha}} = \frac{1}{2} \sum_{m=m_{\alpha}}^{M_{\alpha}} \sum_{\sigma} \left\{ \Psi_{1, m, \sigma}^{\dagger} \begin{pmatrix} -t' & 0 \\ 0 & t' \end{pmatrix} \Psi_{0, m, \sigma} + \text{H.c.} \right\},$$

$$H_{\text{SC}-\text{AM}} = \frac{1}{2} \sum_{m=1}^{W-1} \sum_{\sigma} \left[\left\{ \Psi_{L+1, m, \sigma}^{\dagger} \begin{pmatrix} -t'' & 0 \\ 0 & t'' \end{pmatrix} \Psi_{L, m + \frac{1}{2}, \sigma} + \Psi_{L+1, m+1, \sigma}^{\dagger} \begin{pmatrix} -t'' & 0 \\ 0 & t'' \end{pmatrix} \Psi_{L, m + \frac{1}{2}, \sigma} \right\} + \text{H.c.} \right], \quad (5)$$

respectively, where $(m_1, M_1) = (1, W_n)$ and $(m_2, M_2) = (W - W_n + 1, W)$. In the following calculations, we fix the parameters as $t = t_0 = t_J = t' = t''$, $\mu = -t$, $\Delta = 0.001t$, $\mu_0 = 0$, $W_n = 20$, and $W = 200$. Note that a large exchange potential of $t_J \sim 1\text{eV}$ is expected for RuO_2 [6, 10]. As shown in the Supplemental Material [69], our main conclusions are valid as long as the AM has the distinct

open Fermi surfaces. Furthermore, our conclusions also hold for a device geometry where the normal-metal leads and the SC are on a 45 degree titled square lattice as the AM.

We are interested in the transport properties of the present device. Here, we assume that a bias voltage V_{α} is applied to the lead N_{α} , while the SC is grounded. Within

the Blonder–Tinkham–Klapwijk (BTK) formalism, the time-averaged current in the lead N_α at zero-temperature is calculated by [70, 71]

$$I_\alpha = \sum_{\sigma=\uparrow,\downarrow} I_{\alpha,\sigma}, \quad I_{\alpha,\sigma} = \sum_{\beta=1,2} \int_0^{eV_\beta} G_{\alpha\beta,\sigma} dE, \quad (6)$$

$$G_{\alpha\beta,\sigma} = \frac{e^2}{h} \text{Tr} \left[\delta_{\alpha,\beta} \hat{\mathbb{I}} - \hat{R}_{\alpha\beta,\sigma}^e + \hat{R}_{\alpha\beta,\sigma}^h \right],$$

$$\hat{R}_{\alpha\beta,\sigma}^\nu = \sum_{\sigma'=\uparrow,\downarrow} \hat{s}_{\alpha\beta,\sigma\sigma'}^{\nu e} (\hat{s}_{\alpha\beta,\sigma\sigma'}^{\nu e})^\dagger, \quad (\nu = e, h)$$

where $\hat{\mathbb{I}}$ is the $N_c \times N_c$ identity matrix with N_c representing the number of propagating channels per spin in the normal-metal. The $N_c \times N_c$ matrix of $\hat{s}_{\alpha\beta,\sigma\sigma'}^{ee}$ ($\hat{s}_{\alpha\beta,\sigma\sigma'}^{he}$) contains the scattering coefficients from an electron in the N_β with spin σ' to an electron (hole) in the N_α with spin σ at energy E . We also consider the zero-frequency noise power defined by $C_{\alpha\beta} = \int_{-\infty}^{\infty} \overline{\delta I_\alpha(0) \delta I_\beta(t)} dt$, where $\delta I_\alpha(t) = I_\alpha(t) - I_\alpha$ denotes the deviation of the current at time t from the time averaged current I_α . Within the BTK formalism, the zero-frequency noise power at zero-temperature is calculated by [71, 72]

$$C_{\alpha\beta} = \frac{e^2}{h} \int_0^{eV} P_{\alpha\beta} dE,$$

$$P_{\alpha\beta} = \text{Tr} \left[\delta_{\alpha\beta} \sum_{\nu=e,h} \hat{Q}_{\alpha\alpha}^{\nu\nu} - \sum_{\nu,\nu'} \sigma_\nu \sigma_{\nu'} \hat{Q}_{\alpha\beta}^{\nu\nu'} \hat{Q}_{\beta\alpha}^{\nu'\nu} \right], \quad (7)$$

$$\hat{Q}_{\alpha\beta}^{\nu\nu'} = \sum_{\gamma=1,2} \hat{s}_{\alpha\gamma}^{\nu e} (\hat{s}_{\beta\gamma}^{\nu' e})^\dagger,$$

$$\hat{s}_{\alpha\beta}^{\nu e} = \begin{pmatrix} \hat{s}_{\alpha\beta,\uparrow\uparrow}^{\nu e} & \hat{s}_{\alpha\beta,\uparrow\downarrow}^{\nu e} \\ \hat{s}_{\alpha\beta,\downarrow\uparrow}^{\nu e} & \hat{s}_{\alpha\beta,\downarrow\downarrow}^{\nu e} \end{pmatrix},$$

where $\sigma_\nu = 1$ (-1) for $\nu = e$ (h). In this Letter, we numerically compute the scattering coefficients using the recursive Green's function techniques [73, 74]. Note that the BTK formalism is quantitatively justified for bias voltages well below the superconducting gap.

Results. Before presenting the numerical results, we first give a qualitative description of the characteristic scattering processes in our device. In Fig. 2(a) [Fig. 2(b)], we show the Fermi surfaces of the AM, which are obtained from the Ψ_\uparrow -sector [Ψ_\downarrow -sector] of the Hamiltonian describing electrons with $\sigma = \uparrow$ [\downarrow] and holes with $\sigma = \downarrow$ [\uparrow]. The solid (dashed) lines denotes the Fermi surfaces for the electrons (holes), and the arrows indicate the corresponding group velocity. The spin- σ electrons moving towards the SC segment (i.e., the positive x direction) have the group velocity, $\mathbf{v}_{\sigma,+}^e \propto (\mathbf{x} - s_\sigma \mathbf{y})$. The backward waves of spin- σ electrons and spin- $\bar{\sigma}$ holes have the group velocities, $\mathbf{v}_{\sigma,-}^e \propto (-\mathbf{x} + s_\sigma \mathbf{y})$ and $\mathbf{v}_{\bar{\sigma},-}^h \propto (-\mathbf{x} - s_\sigma \mathbf{y})$, respectively. As a result, we can expect the scattering processes shown in Figs. 2(c)-2(f). First we consider the scattering process of Fig. 2(c), where a spin- \uparrow electron injected from the lead N_1 is scattered at the bottom bound-

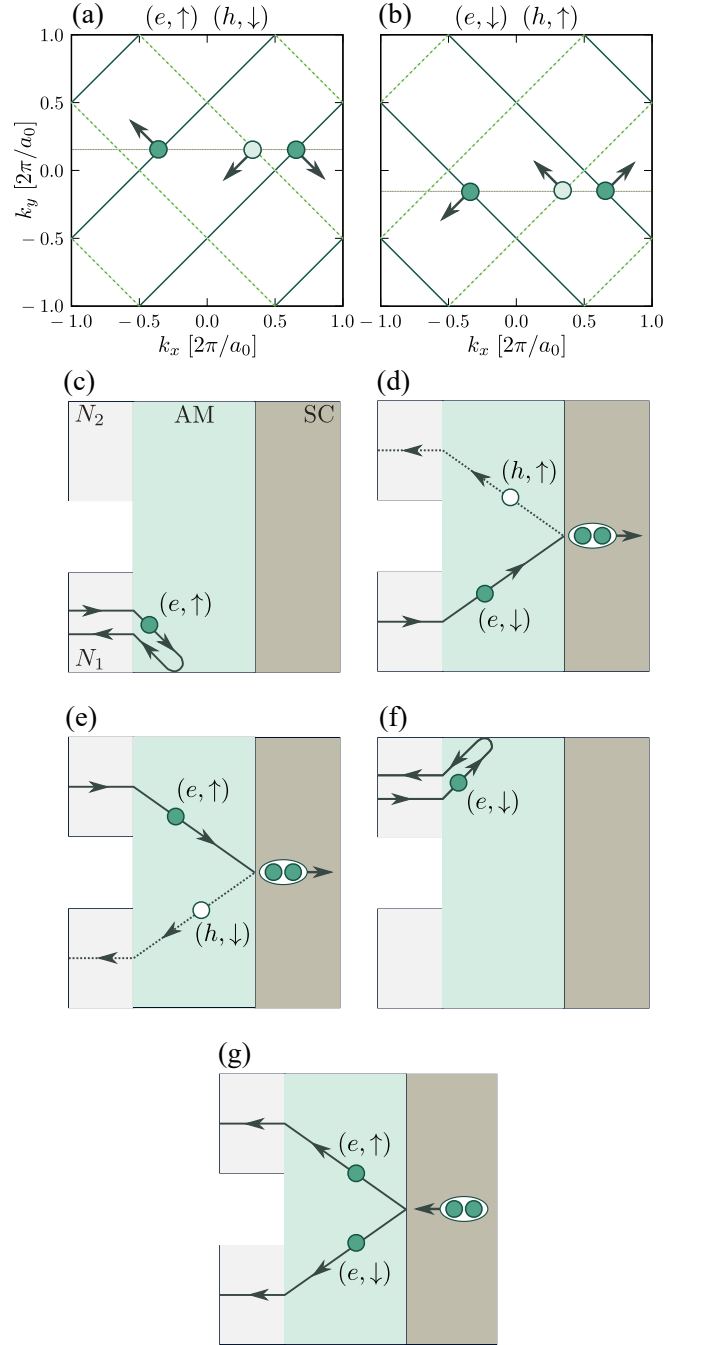


FIG. 2. (a)-(b) Fermi surfaces in the AM. (c)-(f) Scattering processes in the present device. (g) Cooper pair splitting in the present device.

ary of the AM. Since $\mathbf{v}_{\uparrow,+}^e = -\mathbf{v}_{\uparrow,-}^e$, the scattered electron traces back the original trajectory of the incident electron. Therefore, we expect $R_{21,\uparrow}^e = 0$, owing to the retro-reflectivity of *normal* reflections in the AM, where $R_{\alpha\beta,\sigma}^\nu = \text{Tr}[\hat{R}_{\alpha\beta,\sigma}^\nu]$. On the other hand, as illustrated in Fig. 2(d), a spin- \downarrow electron injected from the lead N_1 reaches the AM–SC interface. Since $\mathbf{v}_{\downarrow,+}^e$ and $\mathbf{v}_{\uparrow,-}^h$ differ

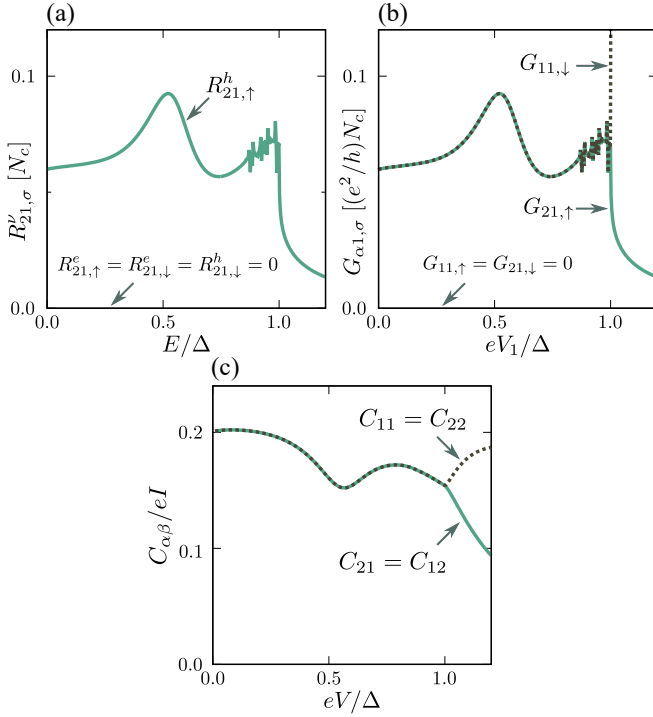


FIG. 3. (a) Scattering amplitudes $R_{21,\sigma}^{\nu}$, where the electrons are injected from the lead N_1 . (b) Differential conductance as a function of the bias voltage eV_1 applied to the lead N_1 , where the lead N_2 is grounded (i.e., $eV_2 = 0$). (c) Zero-frequency noise power as a function of bias voltage, where $eV_1 = eV_2 = eV$.

only in the sign of the x -component, we expect that the incident spin- \downarrow electron undergoes the SAR to the spin- \uparrow hole, which leads to $R_{21,\uparrow}^h \neq 0$. Similarly, for the scattering processes illustrated in Fig. 2(e) and Fig. 2(f), we expect $R_{12,\downarrow}^h \neq 0$ and $R_{12,\downarrow}^e = 0$ due to the SAR and the retro-normal reflection in the AM.

We verify the above expectation by performing numerical simulations, shown in Fig. 3(a). Specifically, we plot $R_{21,\sigma}^{\nu}$ as a function of energy. The length of the AM segment is chosen as $L = 50$. The result is normalized by the number of propagating channels N_c , where $N_c = 14$ with the present parameters. We clearly find that $R_{21,\uparrow}^h \neq 0$, while the amplitudes of other inter-lead scatterings are zero. To detect the characteristic scatterings in experiments, we consider the differential conductance, $G_{\alpha\beta} = dI_{\alpha}/dV_{\beta} = G_{\alpha\beta,\uparrow} + G_{\alpha\beta,\downarrow}$. In Fig. 3(b), we show the differential conductance of $G_{\alpha 1,\sigma}$ as a function of eV_1 , where N_2 is grounded (i.e., $eV_2 = 0$). We find that $G_{11,\downarrow}$ and $G_{21,\uparrow}$ are finite, while other components are zero. Moreover, we obtain $G_{11,\downarrow} = G_{21,\uparrow}$ for $eV < \Delta$ because only the SAR process in Fig. 2(d) contributes to the charge currents. Importantly, the positive non-local conductance of $G_{21,\uparrow}$ is a smoking-gun signature of the dominant SAR [65]. Furthermore, since $G_{11} = G_{11,\downarrow}$

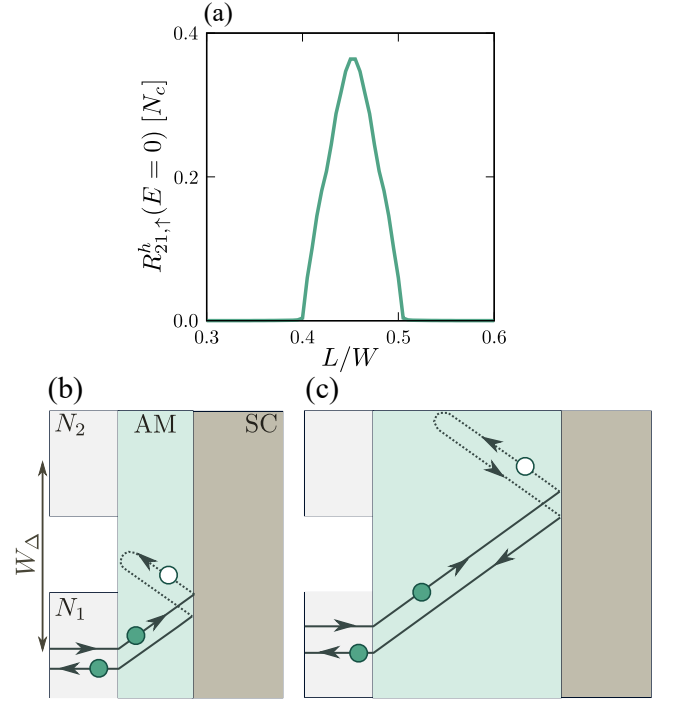


FIG. 4. (a) Scattering amplitudes of $R_{21,\downarrow}^h$ as a function of the length of the AM. (b)–(c) Possible scattering processes that fail to contribute to $R_{21,\downarrow}^h$.

($G_{21} = G_{21,\uparrow}$), we obtain $I_1 = I_{1,\downarrow}$ ($I_2 = I_{2,\uparrow}$). Namely, the charge current in the N_{α} is polarized to \downarrow -spin (\uparrow -spin); by defining the spin current with $I_{\alpha}^s = I_{\alpha,\uparrow} - I_{\alpha,\downarrow}$, we obtain $I_1^s = -I_1$ and $I_2^s = I_2$. Similarly, by applying the bias voltage to the lead N_2 with grounding the lead N_1 , we obtain the \downarrow -spin (\uparrow -spin) polarized currents in the lead N_1 (N_2) due the SAR process in Fig. 2(e).

The time-reversal scattering process of the SAR in the present junction is the Cooper pair splitting as illustrated in Fig. 2(g): a Cooper pair injected from the SC splits into a spin- \downarrow electron flowing into the lead N_1 , while the spin- \uparrow electron flows into the lead N_2 . The positive non-local conductance in Fig. 3(b) is one of the observable signatures for the Cooper pair splitting [65]. Another important signature of the Cooper pair splitting is the positive current cross-correlation [31, 32]. In Fig. 3(c), we show the zero-frequency noise power, $C_{\alpha\beta}$, as a function of the bias voltage, where we apply the same bias voltage to both leads, i.e., $eV_1 = eV_2 = eV$. The results are normalized by $eI = e(I_1 + I_2)$. We clearly find a positive cross-correlation of $C_{12} = C_{21} > 0$. In addition, the relation of $2C_{12} = C_{11} + C_{22}$ holds for $eV < \Delta$, where the cross-correlation in any stochastic process is bounded by the auto-correlation as $2|C_{12}| \leq C_{11} + C_{22}$. Namely, the SAR in the AM induces remarkably strong cross-correlations between the leads.

We discuss the robustness of the SAR in the present

device. In Fig. 4(a), we show $R_{21,\uparrow}^h$ at zero-energy as a function of the length L of the AM. The maximum value of $R_{21,\uparrow}^h$ is taken as $L/W = 0.45$, which corresponds to $L/W_\Delta = 0.5$ with $W_\Delta = W - W_n$ representing the distance between the center of lead N_1 and that of lead N_2 [see also Fig. 4(b)]. This result is intuitively expected from the classical trajectory illustrated in Fig. 2(d). The absence of $R_{21,\uparrow}^h$ for shorter and longer L is also understood by the scattering processes illustrated in Fig. 4(b) and Fig. 4(c). Namely, in the system with too small/large ratio of L/W_Δ , a specularly Andreev reflected hole undergoes the retro-normal reflection at the surface of the AM before reaching the lead N_2 , and eventually returns to the lead N_1 as an electron state. Therefore, the system configuration, especially the ratio of L/W_Δ , is an important factor to observe the SAR in the AM-SC hybrid device.

We also discuss the effect of perturbative Rashba-type spin-orbit coupling (RSOC) [9] described by,

$$H_R = \sum_{\mathbf{r} \in \text{AM}} \sum_{\sigma, \sigma'} (\Lambda_{\mathbf{r}, \sigma, \sigma'} + \text{H.c.}),$$

$$\Lambda_{\mathbf{r}, \sigma, \sigma'} = \sum_{s=\pm} \frac{\lambda}{2i} \{(\mathbf{z} \times \mathbf{d}_s) \cdot \boldsymbol{\sigma}\}_{\sigma\sigma'} c_{\mathbf{r}+\mathbf{d}_s, \sigma}^\dagger c_{\mathbf{r}, \sigma'},$$
(8)

where \mathbf{z} represents the unit vector in the z -direction, $\mathbf{d}_\pm = (\mathbf{x} \pm \mathbf{y})/\sqrt{2}$, and $\boldsymbol{\sigma} = (\sigma_x, \sigma_y, \sigma_z)$ denotes the Pauli matrices in spin space. In Fig. 5(a), we show $G_{\alpha 1, \sigma}(eV = 0)$ as a function of the strength of the RSOC (i.e., λ), where the lead N_2 is grounded. In Fig. 5(b), we show $P_{\alpha\beta}(eV = 0)$ as a function of λ , where the same bias voltage eV is applied to both leads; note that $C_{\alpha\beta} = P_{\alpha\beta}(0)eV$ in the linear response regime. The results in Fig. 5(b) are normalized by $G = \sum_{\alpha, \beta} \sum_{\sigma} G_{\alpha\beta, \sigma}$ at $\lambda = 0$ and $eV = 0$, represented by $G_{\lambda=0}$. The length of the AM is chosen as $L = 50$ in both Fig. 5(a) and Fig. 5(b). The RSOC hybridizes the Ψ_{\uparrow} -states and the Ψ_{\downarrow} -states, and induces spin-flip scatterings that are not listed in Fig. 2. As a result, as shown in Fig. 5(a), we find the appearance of $G_{11,\uparrow}$ and $G_{21,\downarrow}$ with tiny amplitudes and the enhancement of $G_{11,\downarrow}$ due to retro-reflective Andreev reflections (i.e., $R_{11,\downarrow}^h$). Nevertheless, we clearly find that $G_{21,\uparrow}$ has significant positive amplitudes insensitive to λ . The sudden enhancement in the differential conductance at certain λ may be originated from the quantum interference effect, although the details are not clarified. As shown in Fig. 5(b), although the perfect correlation of $2C_{12} = C_{11} + C_{22}$ is smeared, the positive noise cross-correlation also remains insensitive to λ . As a result, we confirm the robustness of correlated spin-currents and Cooper pair splittings against perturbative RSOC.

Summary. In summary, we study the charge transport in a hybrid device consisting of two normal leads, an s -wave SC, and an AM. The particular magnetic nature of the AM causes SARs, which results in the positive nonlo-

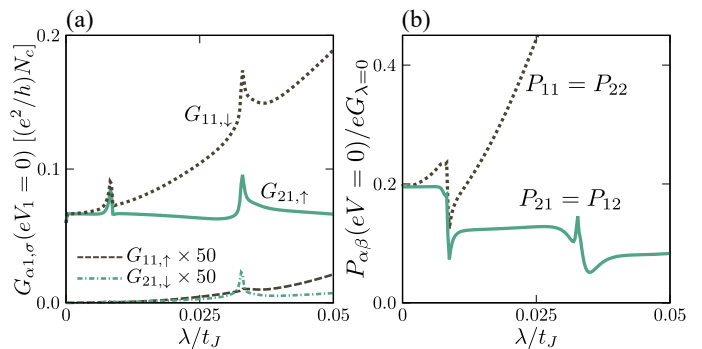


FIG. 5. (a) Differential conductance at zero-bias voltage as a function of the strength of the RSOC. (b) $P_{\alpha\beta} = dC_{\alpha\beta}/dV$ at zero-bias voltage as a function of λ .

cal currents and the positive noise cross-correlations. In conclusion, we propose a new and promising Cooper pair splitter device, which generates highly correlated spin-currents.

S.I. is supported by the Grant-in-Aid for JSPS Fellows (JSPS KAKENHI Grant No. JP22KJ1507).

* These authors contributed equally to this work.

- [1] F. S. Bergeret, A. F. Volkov, and K. B. Efetov, *Rev. Mod. Phys.* **77**, 1321 (2005).
- [2] A. I. Buzdin, *Rev. Mod. Phys.* **77**, 935 (2005).
- [3] J. Linder and J. W. A. Robinson, *Nat. Phys.* **11**, 307 (2015).
- [4] M. Eschrig, *Rep. Prog. Phys.* **78**, 104501 (2015).
- [5] S. Hayami, Y. Yanagi, and H. Kusunose, *J. Phys. Soc. Jpn.* **88**, 123702 (2019).
- [6] L. Šmejkal, R. González-Hernández, T. Jungwirth, and J. Sinova, *Sci. Adv.* **6**, eaaz8809 (2020).
- [7] S. Hayami, Y. Yanagi, and H. Kusunose, *Phys. Rev. B* **102**, 144441 (2020). *Sci. Adv.* **6**, eaaz8809 (2020).
- [8] D.-F. Shao, S.-H. Zhang, M. Li, C.-B. Eom, and E. Y. Tsymlal, *Nat. Commun.* **12**, 7061 (2021).
- [9] L. Šmejkal, A. H. MacDonald, J. Sinova, S. Nakatsuji, and T. Jungwirth, *Nat. Rev. Mater.* **7**, 482 (2022).
- [10] L. Šmejkal, J. Sinova, and T. Jungwirth, *Phys. Rev. X* **12**, 040501 (2022).
- [11] L. Šmejkal, J. Sinova, and T. Jungwirth, *Phys. Rev. X* **12**, 031042 (2022).
- [12] I. Mazin, *Phys. Rev. X* **12**, 040002 (2022).
- [13] X. Zhou, W. Feng, R.-W. Zhang, L. Šmejkal, J. Sinova, Y. Mokrousov, and Y. Yao, *Phys. Rev. Lett.* **132**, 056701 (2024).
- [14] O. Fedchenko, J. Minar, A. Akashdeep, S.W. D'Souza, D. Vasilyev, O. Tkach, L. Odenbreit, Q.L. Nguyen, D. Kutnyakhov, N. Wind, L. Wenthaus, M. Scholz, K. Rossnagel, M. Hoesch, M. Aeschlimann, B. Stadtmueller, M. Klauui, G. Schoenhense, G. Jakob, T. Jungwirth, L. Šmejkal, J. Sinova, H. J. Elmers, *Sci. Adv.* **10**, eadj4883 (2024).
- [15] C. Sun, A. Brataas, and J. Linder, *Phys. Rev. B* **108**,

- 054511 (2023).
- [16] M. Papaj, Phys. Rev. B **108**, L060508 (2023).
- [17] S. Das and A. Soori, arXiv: 2402.08263 (2024).
- [18] S.-B. Zhang, L.-H. Hu, and T. Neupert, arXiv: 2302.13185 (2023).
- [19] H. G. Gilil and J. Linder, arXiv: 2308.10939 (2023).
- [20] A. A. Zyuzin, arXiv: 2402.15459 (2024).
- [21] J. A. Ouassou, A. Brataas, and J. Linder, Phys. Rev. Lett. **131**, 076003 (2023).
- [22] C. W. J. Beenakker and T. Vakhel, Phys. Rev. B **108**, 075425 (2023).
- [23] Q. Cheng and Q.-F. Sun, Phys. Rev. B **109**, 024517 (2024).
- [24] S. Banerjee, M. S. Scheurer, arXiv: 2402.14071 (2024).
- [25] H. G. Gilil, B. Brekke, J. Linder, and A. Brataas, arXiv: 2403.04851 (2024).
- [26] D. Zhu, Z.-Y. Zhuang, Z. Wu, and Z. Yan Phys. Rev. B **108**, 184505 (2023).
- [27] Y.-X. Li and C.-C. Liu, Phys. Rev. B **108**, 205410 (2023).
- [28] B. Brekke, A. Brataas, and A. Sudbø, Phys. Rev. B **108**, 224421 (2023).
- [29] S. A. A. Ghorashi, T. L. Hughes, J. Cano, arXiv: 2306.09413 (2023).
- [30] C. W. J. Beenakker, Rev. Mod. Phys. **80**, 1337 (2008).
- [31] N. M. Chtchelkatchev, G. Blatter, G. B. Lesovik, and T. Martin, Phys. Rev. B **66**, 161320(R) (2002).
- [32] P. Samuelsson, E. V. Sukhorukov, and M. Büttiker, Phys. Rev. Lett. **91**, 157002 (2003).
- [33] J. Cayssol, Phys. Rev. Lett. **100**, 147001 (2008).
- [34] J. J. He, J. Wu, T.-P. Choy, X.-J. Liu, Y. Tanaka, and K. T. Law, Nat. Commun. **5**, 3232 (2014).
- [35] P. Cadden-Zimansky, J. Wei, and V. Chandrasekhar, Nature Phys. **5**, 393 (2009).
- [36] J. Wei and V. Chandrasekhar, Nature Phys. **6**, 494 (2010).
- [37] L. Hofstetter, S. Csonka, A. Baumgartner, G. Fülöp, S. d'Hollosy, J. Nygård, and C. Schönenberger, Phys. Rev. Lett. **107**, 136801 (2011).
- [38] A. Das, Y. Ronen, M. Heiblum, D. Mahalu, A. V. Kretinin, and H. Shtrikman, Nat. Commun. **3**, 1165 (2012).
- [39] J. Schindele, A. Baumgartner, and C. Schönenberger, Phys. Rev. Lett. **109**, 157002 (2012).
- [40] J. Schindele, A. Baumgartner, R. Maurand, M. Weiss, and C. Schönenberger, Phys. Rev. B **89**, 045422 (2014).
- [41] Z. B. Tan, D. Cox, T. Nieminen, P. Lähteenmäki, D. Golubev, G. B. Lesovik, and P. J. Hakonen, Phys. Rev. Lett. **114**, 096602 (2015).
- [42] G. Fülöp, F. Domínguez, S. d'Hollosy, A. Baumgartner, P. Makk, M. H. Madsen, V. A. Guzenko, J. Nygård, C. Schönenberger, A. L. Yeyati, and S. Csonka, Phys. Rev. Lett. **115**, 227003 (2015).
- [43] I. V. Borzenets, Y. Shimazaki, G. F. Jones, M. F. Craciun, S. Russo, M. Yamamoto, and S. Tarucha, Sci. Rep. **6**, 23051 (2016).
- [44] D. Loss and D. P. DiVincenzo, Phys. Rev. A **57**, 120 (1998).
- [45] G. Vidal, Phys. Rev. Lett. **91**, 147902 (2003).
- [46] C. W. J. Beenakker, Phys. Rev. Lett. **97**, 067007 (2006).
- [47] D. Greenbaum, S. Das, G. Schwiete, and P. G. Silvestrov, Phys. Rev. B **75**, 195437 (2007).
- [48] Y. Asano, T. Yoshida, Y. Tanaka, and A. A. Golubov, Phys. Rev. B **78**, 014514 (2008).
- [49] Q. Zhang, D. Fu, B. Wang, R. Zhang, and D. Y. Xing, Phys. Rev. Lett. **101**, 047005 (2008).
- [50] J. Linder, M. Zareyan, and A. Sudbø, Phys. Rev. B **80**, 014513 (2009).
- [51] S.-G. Cheng, Y. Xing, J. Wang, and Q.-F. Sun, Phys. Rev. Lett. **103**, 167003 (2009).
- [52] B. Lv, C. Zhang, and Z. Ma, Phys. Rev. Lett. **108**, 077002 (2012).
- [53] J. Schelter, B. Trauzettel, and P. Recher, Phys. Rev. Lett. **108**, 106603 (2012).
- [54] M. Popinciuc, V. E. Calado, X. L. Liu, A. R. Akhmerov, T. M. Klapwijk, and L. M. K. Vandersypen, Phys. Rev. B **85**, 205404 (2012).
- [55] D. K. Efetov, L. Wang, C. Handschin, K. B. Efetov, J. Shuang, R. Cava, T. Taniguchi, K. Watanabe, J. Hone, C. R. Dean, and P. Kim, Nat. Phys. **12**, 328 (2016).
- [56] M. R. Sahu, P. Raychaudhuri, and A. Das, Phys. Rev. B **94**, 235451 (2016).
- [57] T. Han, J. Shen, N. F. Q. Yuan, J. Lin, Z. Wu, Y. Wu, S. Xu, L. An, G. Long, Y. Wang, R. Lortz, and N. Wang, Phys. Rev. B **97**, 060505(R) (2018).
- [58] P. Pandey, R. Kraft, R. Krupke, D. Beckmann, and R. Danneau, Phys. Rev. B **100**, 165416 (2019).
- [59] P. Ram, D. Beckmann, R. Danneau, and W. Belzig, Phys. Rev. B **108**, 184510 (2023).
- [60] W. Chen, L. Jiang, R. Shen, L. Sheng, B. G. Wang, and D. Y. Xing, Europhys. Lett. **103**, 27006 (2013).
- [61] Z. Hou and Q.-F. Sun, Phys. Rev. B **96**, 155305 (2017).
- [62] Q. Cheng, Z. Hou, and Q.-F. Sun, Phys. Rev. B **101**, 094508 (2020).
- [63] Q. Cheng and Q.-F. Sun, Phys. Rev. B **103**, 144518 (2021).
- [64] L. Majidi and R. Asgari, Phys. Rev. B **93**, 195404 (2016).
- [65] G. Deutscher and D. Feinberg, Appl. Phys. Lett. **76**, 487-489 (2000).
- [66] R. Mélin and D. Feinberg, Eur. Phys. J. B **26**, 101 (2002).
- [67] T. Yamashita, S. Takahashi, and S. Maekawa, Phys. Rev. B **68**, 174504 (2003).
- [68] S. Ikegaya, Y. Asano, and D. Manske, Phys. Rev. Lett. **123**, 207002 (2019).
- [69] Supplemental Material at XXX, which demonstrates the nonlocal charge currents and positive noise cross-correlations with various parameters.
- [70] G. E. Blonder, M. Tinkham, and T. M. Klapwijk, Phys. Rev. B **25**, 4515 (1982).
- [71] M. P. Anantram and S. Datta, Phys. Rev. B **53**, 16390 (1996).
- [72] M. J. M. de Jong and C. W. J. Beenakker, Phys. Rev. B **49**, 16070 (1994).
- [73] P. A. Lee and D. S. Fisher, Phys. Rev. Lett. **47**, 882 (1981).
- [74] T. Ando, Phys. Rev. B **44**, 8017 (1991).

Supplemental Material for “Spin-polarized Specular Andreev Reflections in Altermagnets”

Yutaro Nagae¹, Andreas P. Schnyder², and Satoshi Ikegaya^{1,3}

¹*Department of Applied Physics, Nagoya University, Nagoya 464-8603, Japan*

²*Max-Planck-Institut für Festkörperforschung, Heisenbergstrasse 1, D-70569 Stuttgart, Germany*

³*Institute for Advanced Research, Nagoya University, Nagoya 464-8601, Japan*

We discuss the robustness of the nonlocal charge currents and positive noise cross-correlations in the altermagnet–superconductor hybrid device illustrated in Fig. 1 of the main text. We describe the altermagnet by the Hamiltonian in Eq. (3) of the main text:

$$\begin{aligned}
 H_{\text{AM}} &= \sum_{\mathbf{k}, \sigma} (\varepsilon_{\mathbf{k}} - \mu_0 + s_{\sigma} m_{\mathbf{k}}) c_{\mathbf{k}\sigma}^{\dagger} c_{\mathbf{k}\sigma}, \\
 \varepsilon_{\mathbf{k}} &= 2t_0 \cos \frac{k_x}{2} \cos \frac{k_y}{2}, \quad m_{\mathbf{k}} = 2t_J \sin \frac{k_x}{2} \sin \frac{k_y}{2},
 \end{aligned} \tag{9}$$

where $c_{\mathbf{k}\sigma}^{\dagger}$ ($c_{\mathbf{k}\sigma}$) is the creation (annihilation) operator of an electron with momentum \mathbf{k} and spin σ ; t_0 denotes the nearest-neighbor hopping integral on the square-lattice tilted at 45° with a lattice constant $1/\sqrt{2}$, μ_0 is the chemical potential, and t_J is the strength of the d_{xy} -wave exchange potential. In Figs. 6(a)-6(c) and Figs. 7(a)-7(c), we show the spin-polarized Fermi surfaces with $\mu_0 = t_0 > 0$ and that with $\mu_0 = -t_0 < 0$, respectively. For (a)-(c), the exchange potential t_J is chosen as (a) $t_J = 0.3t_0 < |\mu_0|/2$, (b) $t_J = 0.5t_0 = |\mu_0|/2$, and (c) $t_J = 0.7t_0 > |\mu_0|/2$, respectively. For $2t_J > |\mu_0|$ with $t_J \leq t_0$ and for $2t_0 > |\mu_0|$ with $t_J \geq t_0$, as shown in Fig. 6(c) and Fig. 7(c), the spin- \uparrow [spin- \downarrow] electron has an open Fermi surface along the $(k_x + k_y)$ -direction [$(k_x - k_y)$ -direction]. Otherwise, as shown in Fig. 6(a) and Fig. 7(a), we obtain closed Fermi surfaces surrounding the high-symmetry points of Brillouin zone.

In Fig. 6(c) and Fig. 7(c), we show the ratio of the nonlocal conductance to the local conductance (i.e., G_{21}/G_{11}) at zero-bias voltage (i.e., $eV_1 = 0$) as a function of the exchange potential t_J , where N_2 is grounded (i.e., $eV_2 = 0$). In Fig. 6(d) and Fig. 7(d), we show the ratio of the noise cross-correlation to the noise auto-correlation in the zero-bias voltage limit (i.e., P_{21}/P_{11}) as a function of the exchange potential t_J , where the same bias voltage is applied to both leads. The chemical potential is chosen as $\mu_0 = t_0 > 0$ and that with $\mu_0 = -t_0 < 0$ in Fig. 6 and Fig. 7, respectively. With the closed Fermi surfaces (i.e., $2t_J < |\mu_0|$), G_{21}/G_{11} and P_{21}/P_{11} oscillate and do not always take positive values, which is owing to the coexistence of specular normal reflections and specular Andreev reflections. However, with the open Fermi surfaces (i.e., $2t_J > |\mu_0|$), we always find the positive nonlocal conductance $G_{21} > 0$ and the positive noise cross-correlation $P_{21} > 0$. Moreover, we obtain $G_{21}/G_{11} = 1$ and $P_{21}/P_{11} = 1$ with broad range of t_J , which is due to the dominated specular Andreev reflections. As a result, we demonstrate the robustness of the nonlocal charge currents and positive noise cross-correlations in the presence of the spin-polarized open Fermi surfaces expected in RuO₂.

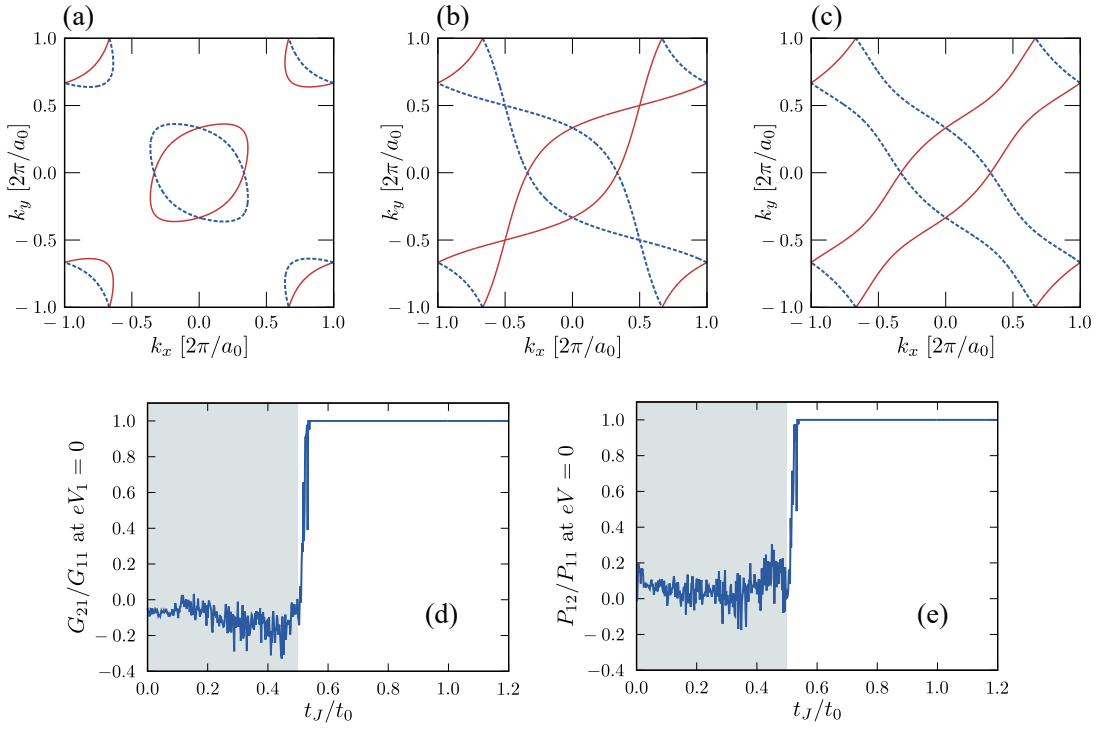


FIG. 6. (a)-(b) Fermi surfaces with $\mu_0 = t_0 > 0$, where the exchange potential is chosen as (a) $t_J = 0.3t_0 < |\mu_0|/2$, (b) $t_J = 0.5t_0 = |\mu_0|/2$, and (c) $t_J = 0.7t_0 > |\mu_0|/2$, respectively. The solid (dashed) line denotes the Fermi surface for the spin- \uparrow (spin- \downarrow) electron. (c) Ratio of the nonlocal conductance to the local conductance at zero-bias voltage as a function of the exchange potential t_J . (d) Ratio of the noise cross-correlation to the noise auto-correlation in the zero-bias voltage limit (i.e., P_{21}/P_{11}) as a function of the exchange potential t_J . In (c) and (d), the chemical potential is chosen as $\mu_0 = t_0$, and the shaded region represents $2t_J < \mu_0$.

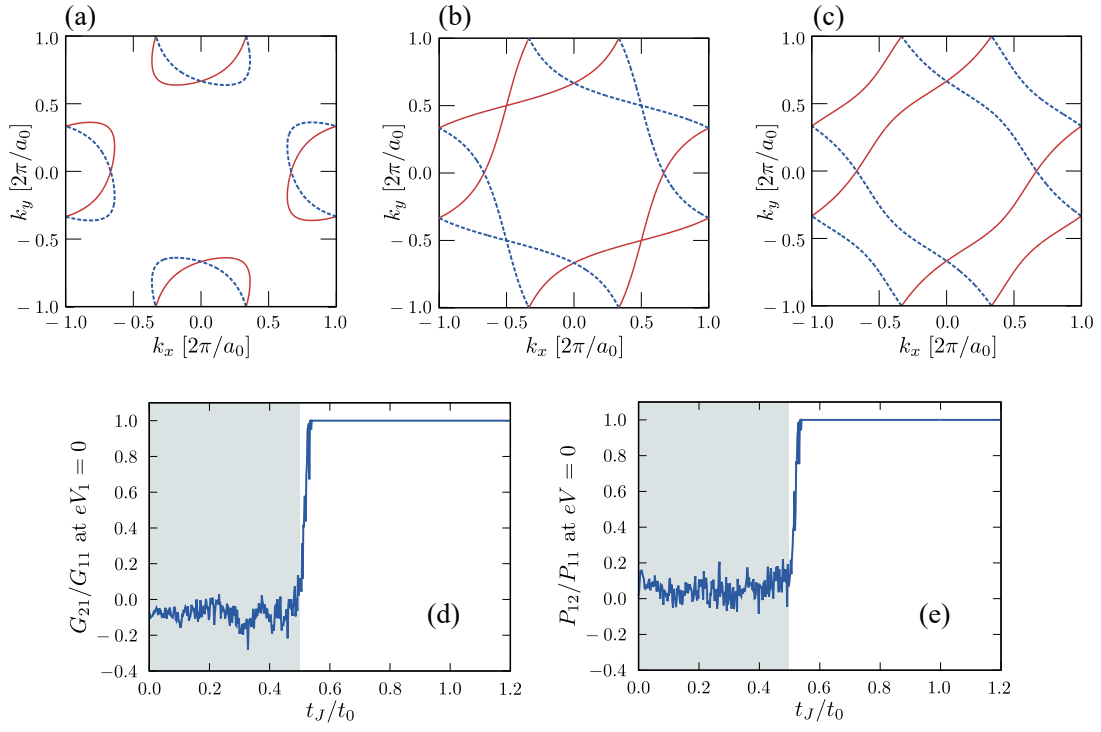


FIG. 7. (a)-(b) Fermi surfaces with $\mu_0 = -t_0 < 0$, where the exchange potential is chosen as (a) $t_J = 0.3t_0 < |\mu_0|/2$, (b) $t_J = 0.5t_0 = |\mu_0|/2$, and (c) $t_J = 0.7t_0 > |\mu_0|/2$, respectively. The solid (dashed) line denotes the Fermi surface for the spin- \uparrow (spin- \downarrow) electron. (c) Ratio of the nonlocal conductance to the local conductance at zero-bias voltage as a function of the exchange potential t_J . (d) Ratio of the noise cross-correlation to the noise auto-correlation in the zero-bias voltage limit (i.e., P_{21}/P_{11}) as a function of the exchange potential t_J . In (c) and (d), the chemical potential is chosen as $\mu_0 = -t_0$, and the shaded region represents $2t_J < |\mu_0|$.